Accepted for publication in The Astrophysical Journal
Preprint typeset using LaTeX style emulateapj v. 11/26/04

ON THE EVOLUTION OF THERMONUCLEAR FLAMES ON LARGE SCALES

Ju Zhang[1,2], O. E. Bronson Messer[1,2,3], Alexei M. Khokhlov[1,2] and Tomasz Plewa[1,2]

Accepted for publication in The Astrophysical Journal

ABSTRACT

The thermonuclear explosion of a massive white dwarf in a Type Ia supernova explosion is characterized by vastly disparate spatial and temporal scales. The extreme dynamic range inherent to the problem prevents the use of direct numerical simulation and forces modelers to resort to subgrid models to describe physical processes taking place on unresolved scales.

We consider the evolution of a model thermonuclear flame in a constant gravitational field on a periodic domain. The gravitational acceleration is aligned with the overall direction of the flame propagation, making the flame surface subject to the Rayleigh-Taylor instability. The flame evolution is followed through an extended initial transient phase well into the steady-state regime. The properties of the evolution of flame surface are examined. We confirm the form of the governing equation of the evolution suggested by Khokhlov (1995).

The mechanism of vorticity production and the interaction between vortices and the flame surface are discussed. Previously observed periodic behavior of the flame evolution is reproduced and is found to be caused by the turnover of the largest eddies. The characteristic timescales are found to be similar to the turnover time of these eddies. Relations between flame surface creation and destruction processes and basic characteristics of the flow are discussed. We find that the flame surface creation strength is associated with the Rayleigh-Taylor time scale. Also, in fully-developed turbulence, the flame surface destruction strength scales as $1/L^3$, where L is the turbulent driving scale.

The results of our investigation provide support for Khokhlov's self-regulating model of turbulent thermonuclear flames (Khokhlov 1995). Based on these results, one can revise and extend the original model. The revision uses a local description of the flame surface enhancement and the evolution of the flame surface since the onset of turbulence, rendering it free from the assumption of an instantaneous steady state of turbulence. This new model can be applied to the initial transient phase of the flame evolution, where the self-regulation mechanism yet to be fully established. Details of this new model will be presented in a forthcoming paper.

Subject headings: supernovae: general – turbulence

1. INTRODUCTION

Thermonuclear combustion was originally proposed as the mechanism behind Type Ia supernovae (Hoyle & Fowler 1960; Arnett 1969). However, this detonation-based model was soon shown to be unable to explain a host of observations (Arnett 1974; Ostriker, Richstone, & Thuan 1974). Nomoto, Sugimoto, & Neo (1976) recognized the possibility that a deflagration, a subsonic mode of combustion following a mild ignition of stellar material in the center of a massive white dwarf, might help to ameliorate these deficiencies. Flames characteristic of a deflagration are subject to the Rayleigh-Taylor instability in the gravitational field in the interior of a white dwarf, significantly complicating any detailed calculation of this mode of burning.

The parameterized one-dimensional study of Nomoto, Thielemann, & Yokoi (1984) indicated that a successful explosion model may require a substantial increase in the speed of the deflagrating front. Such an increase in burning speed was observed in the multi-dimensional models of Müller & Arnett (1982, 1986), though Müller & Arnett (1986) recognized that their models lacked a proper description of turbulence (and also lacked details of the microphysics) taking place on scales unresolved in their simulations.

The structure and dynamics of deflagration fronts on Rayleigh-Taylor-dominated scales were studied in detail by Khokhlov (1995). In particular, Khokhlov proposed that when a steady state of fully-devloped turbulence is assumed, the evolution of the flame propagation becomes independent of details of the microphysics and is governed by a self-regulating mechanism reflecting an interplay between the Rayleigh-Taylor instability and nuclear burning. Khokhlov (1995) provides scaling relations for the turbulent flame speed and these scalings are used to construct a subgrid-scale (SGS) model which, combined with a flame capturing scheme, offers a powerful tool for studying deflagrations in Type Ia supernovae.

The use of subgrid-scale models in modeling of Type Ia supernovae is necessitated by the vastly disparate temporal and spatial scales present in the problem. Without exception, all groups involved in studying thermonuclear supernovae use some sort of subgrid-scale model. In the Khokhlov self-regulation scenario, the turbulent flame speed is primarily determined by the speed of large-scale motions driven by the Rayleigh-Taylor instability. This speed is $\propto \sqrt{AgL}$, where A is the Atwood number, g is the local gravitational acceleration, and L is the driving scale. In this subgrid model, it is assumed that a steady

[1] Center for Astrophysical Thermonuclear Flashes, The University of Chicago, Chicago, IL 60637
[2] Department of Astronomy & Astrophysics, The University of Chicago, Chicago, IL 60637
[3] present address: National Center for Computational Sciences, Oak Ridge National Laboratory, Oak Ridge, TN 37831

state of fully-developed turbulence obtains instantaneously, leading to a state of self regulation where the interplay of the RT instability and the local progress of the flame serves to render the turbulent flame speed roughly constant in time. However, the model does not take into account the initial transient phase nor the unsteadiness of local turbulent velocities. The subgrid model of Niemeyer & Hillebrandt (1995) uses the framework of Kolmogorov turbulence theory as a starting point. In their model, the burning speed is locally determined from the turbulent kinetic energy, k_{sgs}, which is evolved through the use of a local transport equation (Clement 1993). This model has been used extensively to study thermonuclear deflagrations both without (Niemeyer, Hillebrandt, & Woosley 1996) and, later, with (Reinecke, Hillebrandt, & Niemeyer 1999, 2002) a flame front tracking scheme. Despite the fundamental differences in these subgrid models, the results obtained (explosion energetics, timescale, and ejecta morphology) are quite similar for deflagrations in the self-regulation regime (Reinecke, Hillebrandt, & Niemeyer 1999, 2002; Gamezo et al. 2003; Schmidt, Niemeyer, Hillebrandt, & Röpke 2006). Accordingly, we can conclude that in the self-regulation regime differences between specific subgrid models do not lead to gross differences in the flame evolution.

Our aim here is to improve the original Khokhlov subgrid-scale model (hereafter KSGS) and develop a new subgrid model that can be applied not only to the self-regulation regime but also to the initial transient phase before self regulation has been fully established. The inclusion of a description of this transient phase in the subgrid model is especially important for the simulation of the early evolution of deflagrations in Type Ia supernovae.

To develop the new subgrid model, we have first conducted a survey of thermonuclear model flame simulations on periodic domains. These results allow us to develop a deeper understanding of the flame dynamics on small scales and provide a foundation for the improved scheme.

2. NUMERICAL METHODS AND MODELS

In our study of model thermonuclear flames, we consider the evolution of the reactive Eulerian equations in Cartesian geometry. Numerical solutions were obtained with the FLASH code (Fryxell et al. 2000). The majority of the models presented here were computed in three-dimensions, while a limited number of models have been calculated in two-dimensions.

2.1. *Numerical Methods*

We assume a constant gravitational acceleration, g_z, aligned with and pointing along the negative z coordinate. The computational domain is a tube (a channel in 2D) with square cross-section. We use periodic boundary conditions along the lateral (i.e. (x, y)) directions. We impose reflecting boundary conditions at the bottom of the tube, while allowing outflow through its top boundary. The time steps in our simulation were limited with Courant factor of 0.6.

In order to save computational resources, we use FLASH's adaptive mesh refinement (AMR) capability and only resolve regions actively participating in combustion. In these regions, we track flow structures characterized by large jumps in density, total velocity, or progress variable.

At the initial time, a one-dimensional flame front structure is interpolated onto the grid with the flame front position, z_f, defined as

$$z_f = z_0 + A_f \cos(2\pi x/\lambda_x)\cos(2\pi y/\lambda_y)\,,$$

where z_0 is the unperturbed position of the front, A_f is the amplitude of the perturbation, and $\lambda_x = \lambda_y = \lambda$ is the wavelength of the perturbation in the lateral directions. The fuel filling the tube ahead of the flame front is initially at rest and composed entirely of equal mass fractions of carbon and oxygen. The fuel's density is 1×10^8 g/cm^3 and its temperature is $5 \times 10^7 K$. We consider here only a one-step reaction in the burning front with a constant prescribed energy release of 7×10^{17} erg/g (i.e. the total energy that would be released in taking the initial carbon-oxygen mix to a composition of all iron). We use a Helmholtz equation of state (Timmes & Swesty 2000) suitable for the degenerate conditions considered here.

The original FLASH code has been equipped with a custom implementation of the flame-capturing algorithm of Khokhlov (1995); Gamezo et al. (2003). In this framework, the flame front is described as a diffuse, thick interface of a progress variable, f, whose evolution is governed by an advection-diffusion-reaction (ADR) equation:

$$\frac{\partial f}{\partial t} + U \cdot \nabla f = K\nabla^2 f + R\,, \tag{1}$$

Here f is constrained to lie between $f = 0$ (unburned material, or fuel) and $f = 1$ (completely burned material, or ash). The diffusion and reaction coefficients, K and R, are given by

$$K = \text{const},$$
$$R = \begin{cases} C = \text{const}, & \text{if } f_0 \le f \le 1\,, \\ 0, & \text{otherwise}\,, \end{cases}$$

where $f_0 = 0.3$. Equation (1) describes a reactive front of thickness $\delta \simeq (K/C)^{1/2}$ propagating with the speed $D = (KC/f_0)^{1/2}$. With coefficients K and C defined as

$$K = D(\beta\Delta x)\sqrt{f_0},\ C = \frac{D}{(\beta\Delta x)}\sqrt{f_0},$$

and $\beta = 1.5$, the front diffuses with a prescribed constant speed D and spreads over $\approx 3 - 4$ zones. For the advection part of the ADR scheme we use the PPM (Colella & Woodward 1984) solver in FLASH. For a more detailed description of the flame-capturing method and its characteristics see Khokhlov (1995) and Zhiglo (2005). Verification of the FLASH implementation of this scheme has been presented in Vladimirova, Weirs, & Ryzhik (2006).

2.2. *Database of Numerical Models*

In order to gain insight into the nature of the evolution of turbulent thermonuclear flames on large scales, we have constructed an extensive database of numerical flame models.

Tables 1 and 2 provides a complete list of the catalogued simulations.

TABLE 1
Model Turbulent Thermonuclear Flames

Parameter	Definition
$N_x \times N_y \times N_z$	model resolution [a]
L	lateral extent of the computational domain
D_l	laminar flame speed
D_t	turbulent flame speed
g_z	gravitational acceleration
Fr	Froude number, $Fr = D_l^2/g_z L$
A_f	amplitude of the flame front perturbation in vertical direction
λ	wavelength of the flame front perturbation in lateral directions
b	nominal numerical thickness of the flame front (number of computational cells)

[a]Effective resolution of AMR model.

TABLE 2
High-Resolution non-SGS Models[a]

Model	$N_x \times N_y \times N_z$	L [cm]	Δx [cm]	D_l [cm s^{-1}]	g_z [cm s^{-2}]	$Fr \times 10^4$	b
R1	$64 \times 64 \times 2560$	1.5×10^6	2.34×10^4	1.07×10^6	1.9×10^9	4.02	4
R2	$128 \times 128 \times 5120$	1.5×10^6	1.17×10^4	1.07×10^6	1.9×10^9	4.02	4
R3	$256 \times 256 \times 10240$	1.5×10^6	5.86×10^3	1.07×10^6	1.9×10^9	4.02	4
BH	$128 \times 128 \times 5120$	1.5×10^6	1.17×10^4	1.07×10^6	1.9×10^9	4.02	3
B2	$128 \times 128 \times 5120$	1.5×10^6	1.17×10^4	1.07×10^6	1.9×10^9	4.02	6
DH	$64 \times 64 \times 2560$	1.5×10^6	2.34×10^4	0.54×10^6	1.9×10^9	1.01	4
D2	$64 \times 64 \times 2560$	1.5×10^6	2.34×10^4	2.14×10^6	1.9×10^9	16.1	4
LH	$64 \times 64 \times 2560$	0.75×10^6	2.34×10^4	1.07×10^6	1.9×10^9	8.04	4
L2	$128 \times 128 \times 5120$	3.0×10^6	1.17×10^4	1.07×10^6	1.9×10^9	2.01	4
GH	$64 \times 64 \times 2560$	1.5×10^6	2.34×10^4	1.07×10^6	9.5×10^8	8.04	4

[a]$A_f = 9.96 \times 10^4 cm$, $\lambda = 4.46 \times 10^5 cm$.

Our high resolution models are primarily intended to extend the simulations of Khokhlov (1995), verify our implementation of the flame capturing algorithm, verify the KSGS model, and demonstrate numerical convergence. Specifically, models R1, R2 and R3 are used to investigate grid convergence. Models BH and B2 together with model R2 are used to demonstrate the insensitivity of the results to the numerical flame thicknesses, b. Models DH, R1 and D2 are used in a discussion of flame dynamics, including the self-regulation mechanism. In models LH, R1 and L2 we vary the size of computational domain. These models are analized in our study of the flame destruction process. Models R1, D2, GH and L2, having various domain sizes and the imposed gravitational accelerations, are used to verify the KSGS model.

3. FLAME DYNAMICS

Following Damköhler (1939, see also Khokhlov (1995); Niemeyer & Hillebrandt (1995)), a primary consequence of turbulence is to increase the flame surface area. The turbulent flame speed is,

$$D_t = \rho_0^{-1} \frac{dM_b}{dt} ,$$

where the burned mass, M_b, is normalized to the area of the unperturbed flame the horizontal cross-section of the computational domain. The turbulent flame speed is expected to vary in proportion to the surface area, S, as

$$D_t = \frac{S}{S_0} D_l , \qquad (2)$$

where S_0 is the surface area of an unperturbed flame. Khokhlov (1995) suggested, based on examination of simple flame surface geometries, that the evolution of the flame surface area can be described as a competition between flame surface creation and destruction processes:

$$\frac{dS}{dt} = cS - dD_l S^2 , \qquad (3)$$

where

$$c = [(\mathbf{e}_1)_i (\mathbf{e}_1)_j + (\mathbf{e}_2)_i (\mathbf{e}_2)_j] (\frac{\partial U_i}{\partial x_j}). \qquad (4)$$

Here $(\mathbf{e}_{1,2})_i$ are two orthonormal vectors tangent to an infinitesimal surface element δS. The first unit vector, $\mathbf{e}_1$, is orthogonal to vector normal to the flame surface, $\mathbf{n} = \nabla f / |\nabla f|$, and is chosen arbitrarily; the second unit vector, $\mathbf{e}_2$, is orthogonal to both $\mathbf{e}_1$ and $\mathbf{n}$ and is then determined uniquely.

The first term on the right-hand side of Eq. (3) describes surface creation by strain, while the second term in this equation represents the process of flame surface destruction due to the propagation of cusps. In steady state, the two terms balance one another in a statistical sense. Then, $S \propto D_l^{-1}$ follows from Eq. (3) implying that the turbulent flame speed D_t is independent of the laminar flame speed, D_l.

Each term in Eq. (3) can be calculated using available information from our simulations. The flame surface area, S, is extracted from the data as an iso-surface of the progress variable at $f = 0.5$ using a marching-cube algorithm (Lorensen & Cline 1987). The computational cells that contain flame surface (defined by $f = 0.5$) are then used to calculate the surface creation coefficient, c: First, a unit vector normal to the flame surface, $\mathbf{n}$, is calculated. Then two unit vectors, $\mathbf{e}_1$ and $\mathbf{e}_2$, orthogonal to $\mathbf{n}$ and to each other are constructed (Khokhlov 1995). It is the average value of the creation coefficient that is followed, $\int_\Omega c dV / \int_\Omega dV$, where Ω is the volume

containing flame surface, *i. e.* all of the computational cells that contain flame surface. The total flame surface area, S, and creation term, cS, are computed by integrating over the entire flame surface with $S = \int_\Omega dS$ and $cS = \int_\Omega cdS$. The total destruction term is then calculated as the difference between total creation and dS/dt, where dS/dt is simply calculated by finite differencing in time.

3.1. *Flame Surface Evolution*

We begin with an examination of the evolution of the model flames listed in Tables 1 and 2. These results serve as the basis for the analysis of the actual form of the governing equation for flame surface evolution. First, we examine the evolution of models with different laminar flame speeds, D_l. These results are closely associated with the self-regulation mechanism that will be discussed throughout this paper. Fig. 1

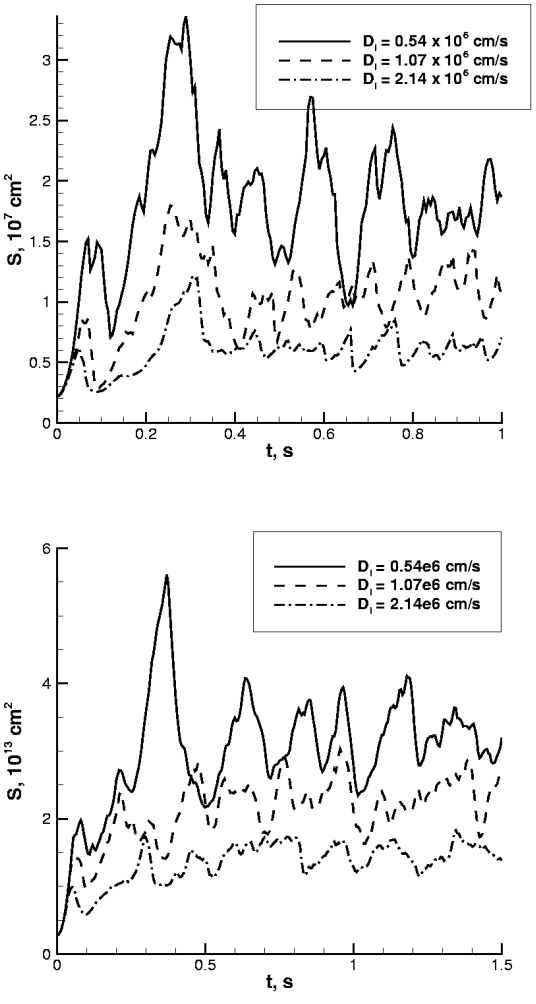

FIG. 1.— Temporal evolution of flame surface area in 2D (top) and 3D (bottom). Note that in 2D, the models are the counterparts of models DH, R1 and D2 in 3D.

shows the evolution of the flame surface area at three different laminar flame speeds both in 2D and 3D. It is expected that the larger the laminar flame speed, the smaller the flame surface. As discussed by Khokhlov (1995) and shown in Sec. 3.5, the larger the laminar flame speed, the stronger the smoothing effect due to burning, thus the smaller the flame surface area.

TABLE 3
STATISTICS OF FLAME SURFACE IN STEADY STATE

D_l $\times 1.07 \times 10^{-6}$ cm/s (2D)	$\bar{S}$ $\times 10^{-7}$ cm^2	S' $\times 10^{-7}$ cm^2
0.5	1.8	0.9
1.	1.	0.5
2.	0.5	0.3
D_l $\times 1.07 \times 10^{-6}$ cm/s (3D)	$\bar{S}$ $\times 10^{-13}$ cm^2	S' $\times 10^{-13}$ cm^2
0.5.	3.2	1.2
1.	2.5	1
2.	1.2	0.5

Even a crude inspection of Fig. 1 suggests that a steady state exists and the flame exhibits a semi-periodic behavior about this equilibrium.[4] The time averaged value and the standard deviation of the flame surface area in steady state (at t > 0.6 s) are listed in Table 3.

Both the time averaged value and the standard deviation of the flame surface area appear to scale as D_l^{-1}. In most cases considered this relation is fulfilled with accuracy of $\approx 10\%$. Following our trial time-limited high-resolution runs, this agreement seems improving with increased resolution. Both the time averaged turbulent flame speed and its deviation are independent of the laminar flame speed. This is in agreement with Eq. (2) and is illustrated in Fig. 2.

Therefore, our study confirms the independence of the turbulent flame speed and the laminar flame speed. This is the essential property of the self-regulation mechanism discussed by Khokhlov (1995). However, the independence of the deviation of turbulent flame speed versus laminar flame speed has not been discussed in that previous study.

3.2. *Character of The Steady State*

As discussed in the previous section, the flame exhibits a semi-periodic behavior once a steady state is established. A natural question then is "What is the source of the oscillation?" It is conceivable that the oscillation is caused by interference between the flame and acoustic waves generated at the bottom wall boundary. On the other hand, it could be an intrinsic property of Rayleigh-Taylor unstable flames. In order to determine whether of these hypotheses is likely we perform a 1D test without flame propagation. In this test an initial vertical downward velocity is imposed on the fluid and the propagation of sound waves generated at the bottom wall is examined. We find that the sound waves quickly reach the top boundary and leave the computational domain. The fluid becomes essentially at rest once the sound wave propagates off the grid. In addition, a simulation of flame propagation in 2D with both the top and bottom boundaries open have been performed and the same semi-periodic behavior found in our fiducial models is observed.

On the basis of these experiments, we conclude that flames subject to the Rayleigh-Taylor instability are intrinsically oscillatory. In 2D, the rising bubbles filled

[4] The character of the steady state will be further elaborated in Sec. 3.2.

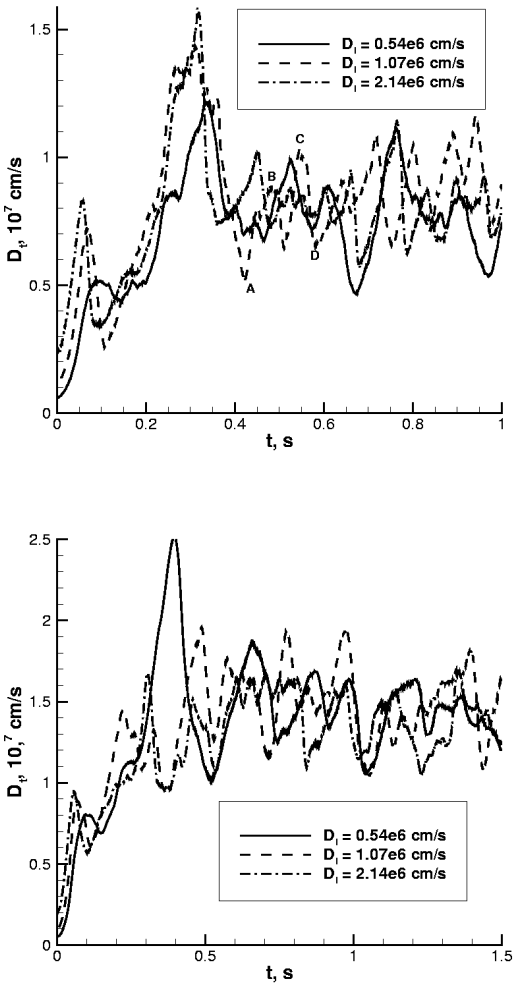

FIG. 2.— Evolution of the turbulent flame speed, D_t in 2D (left) and 3D (right) in models DH (solid line), R1 (dashed line) and D2 (dash-dotted line). Note that a statistically steady-state evolution is preceded by an extended transient. The time-averaged turbulent flame speed does not depend on the laminar flame speed once a steady-state regime is established, where the evolution is governed by the self-regulation of the flame surface.

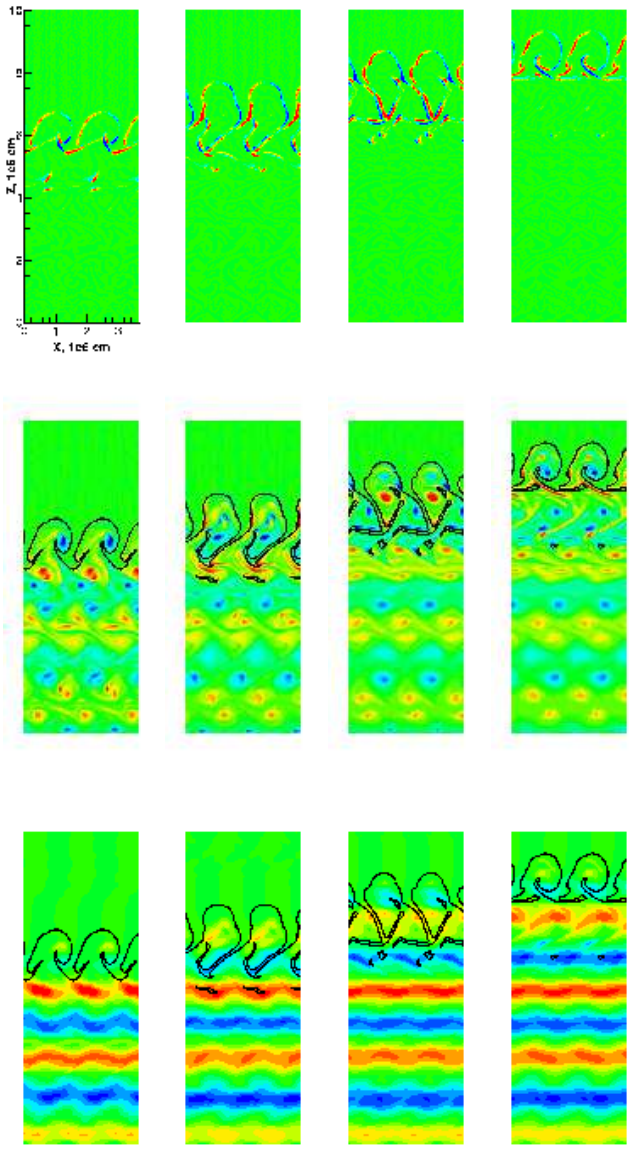

FIG. 3.— Evolution of a turbulent flame in two-dimensions in statistical steady state. Shown is the distribution of vorticity generation, $\nabla\rho \times \nabla p$ (top row), vorticity (middle row) and horizontal velocity (bottom row) at four different instants of time (from left to right: 0.41, 0.47, 0.54 and 0.58 s, corresponding to "A" - "D" marked in the first panel of Fig. 2). Each row covers about two eddy turnover times (~ 0.2 s). Each panel is a lateral composite of 2.5 of our periodic domains, arranged for visualization purposes.

with hot burned material are analogous to a cylinder passing through a fluid. It is well known that this schematic situation typically results in the formation of a vortex street in the wake of the cylinder (White 2003). Similarly, a vortex street also appears in the wake of the flame front in our simulations, and the periodicity of the structure is apparent in Fig. 3.

The production of vorticity (top panels in Fig. 3) is caused by the misalignment of the density and pressure gradients at the sides of the flame bubbles. The pressure gradient tends to be oriented along the direction of gravity, whereas the density gradient is approximately normal to the flame surface. Vortices are formed and then shed from the flame surface (middle panels in Fig. 3). The vortices turn over, stretch and fold the flame surface near the tail (panels for 0.47 and 0.54 s). These stretched and folded surfaces then collide and annihilate. During this process, the heads of the bubbles wobble and their tails swing from side to side. Approximately one full period of this "wobbling" process is shown in Fig. 3. During each oscillation period, two eddies of opposite direction are shed from the surface of each bubble. One such turnover is illustrated in Fig. 4.

The size of the eddies is comparable to the turbulent driving scale, L, *i.e.* the domain width.

Each flame wobble is characterized by varying flame surface resulting in variations of the turbulent flame speed. For example, consider two maxima of the turbulent flame speed marked "B" and "C" in the top panel of Fig. 2 (2D model with $D_l = 1.07e6$ cm/s). The flame structure corresponding to these two extrema is illus-

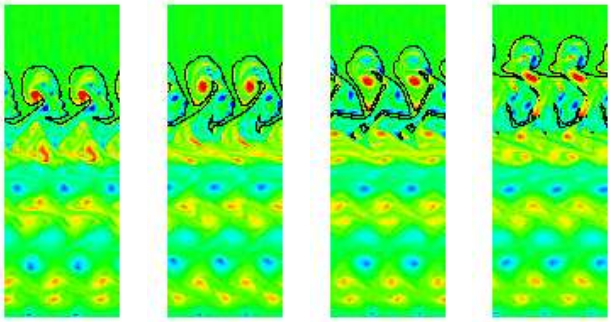

FIG. 4.— Eddy turnover in a turbulent flame in two-dimensions. Plotted is the vorticity distribution. Note the counter-clockwise rotating eddy (the red "blob"-like feature inside the bubble) as it stretches and folds the flame surface near the tail. Axes are the same as those in Fig. 3.

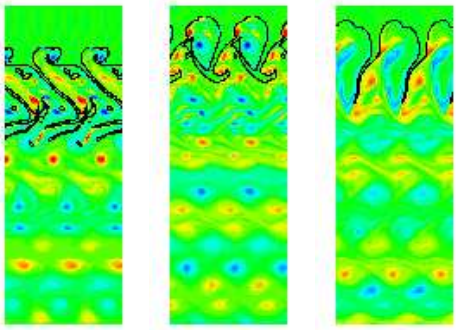

FIG. 5.— Vorticity distributions in steady state. Laminar flame speeds are (from left to right): 0.54e6 cm/s, 1.07e6 cm/s and 2.14e6 cm/s corresponding to the three 2D runs shown in Fig. 1. The scale of the axes are kept the same in each panel. The vertical wavelengths are approximately the same, being about twice as large as the domain width. Note, again, each panel has been duplicated horizontally 2.5 times and axes are the same as those in Fig. 3.

trated in the second and the third column in Fig. 3. Note that, at these two instants of time, the flame surface area is also at its largest, as indicated by extreme length of the bubble's tail.

The above picture is in qualitative agreement with the recent two-dimensional study of Vladimirova & Rosner (2005) obtained in the Boussinesq limit. In particular, the morphology of the flame and the formation of vortex streets are common features of the two models [see (Vladimirova & Rosner 2005), panels (a), (e), and (f) in Fig. 1]. Note that in their simulations with symmetric boundaries, no oscillatory behavior is observed. We consider this to be an effect of the symmetric boundary conditions. In reality, there is no imposed symmetry and the RT flame is physically periodic as a result of eddy turnover. It should be pointed out the horizontal reflecting boundary they sometimes term a symmetric boundary should not be confused with a wall boundary. Here, we observe periodic behavior also in the flame evolution with horizontal wall boundaries. In addition, Vladimirova & Rosner (2005) surprisingly find that the ratio of the vertical wavelength and the domain width is invariant and always close to 2. A similar result is obtained here (Fig. 5) for which we offer the following explanation:

As mentioned above, in steady state, the largest RT unstable structure is always comparable to the turbulent driving scale of the system. Since the periodicity is caused by the turnover of these largest eddies, and there are two turnovers in each period, it is natural that the vertical wavelength is always about twice as large as the domain width.

The character of the steady state has been discussed in the context of 2D simulations in the above. In 3D, although vortices shed from the flame surface do not merge into the bulk but cascade into smaller and smaller structures, and the flame surface is not as regular (Fig. 6),

the overall mechanism of vorticity production near the flame front and the subsequent interaction between vortices and the flame surface is similar to that observed in 2D. Regarding vorticity generation, vortex stretching is an important contributing mechanism of vorticty generation uniquely present in 3D. While vortex stretching is a dominant source of vorticity in the bulk, its strength

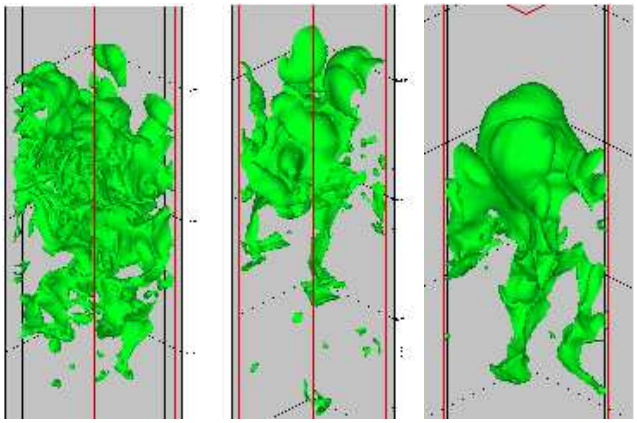

FIG. 6.— Morphology of the turbulent flame surface in models with different laminar flame speeds at late times. (left): model DH, $D_l = 0.54 \times 10^6$ cm/s; (middle): model R1, $D_l = 1.07 \times 10^6$ cm/s; (right) model D2, $D_l = 2.14 \times 10^6$ cm/s. Note the larger the laminar flame speed, the smoother and, concomitantly, the smaller the flame surface. The vertical spatial scale are 1×10^7 to 1.6×10^7, 0.7×10^7 to 1.35×10^7 and 1.2×10^7 to 1.8×10^7 cm for model DH, R1 and D2, respectively.

is comparable to that of barcolinic vorticity generation near the flame surface. The latter mechanism is common to 2D and 3D and is the original source of vorticity in our problem.

In addition, the same semi-periodic behavior is also observed in 3D flame evolution, as can be seen in Fig. 2. Just as in 2D, this semi-periodic behavior is caused by the turnover of largest eddies. Despite the complicated structure of a 3D flame, the periodically layered structure can still be discerned in a 2D slice of the 3D flow by coarsening the grid by a factor of 16. Such slices are shown in Fig. 7.

To actually extract the period of the temporal evolution of the flame, the run shown in (Fig. 2) was analyzed for $t \geq 0.6$ s in both 2D and 3D. Figure 8 shows the results of the analysis obtained for 3D with the help of the CLEAN method (Roberts, Lehard, & Dreher 1987) for power spectrum analysis, together with the results

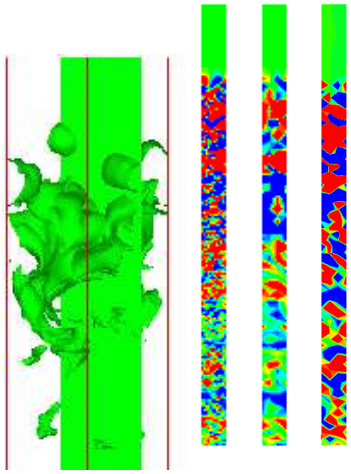

FIG. 7.— Turbulent flame at ∼0.83 s for model R1. The 3D flame surface and the position of the 2D slice are shown in the first panel. Only that part of the domain that contains the flame (vertical spatial scale from 1×10^7 to 1.6×10^7 cm) is shown in this first panel. The second panel plots the horizontal velocity field (component in the plane) in the 2D slice. The 3rd and 4th panel show the horizontal velocity field and the vorticity (normal to the plane) on the coarsened grid. Note the trace of the layered structure in these two panels. (N.B. In contrast to the 3D plot, the slices cover the entire domain height from 0 to 3×10^7 cm.)

obtained by computing the auto-correlation of the time series D_t (at $t \geq 0.6\,\mathrm{s}$) in Fig. 2 , *i.e.* the correlation of $D_t(t)$ against a time-shifted (by τ) version of it. Fig. 8 shows that both methods indicate the presence of excess power around $0.2s$. In particular, there is a clear accumulation of power for frequencies $< 10\ \mathrm{s}^{-1}$ in the power spectrum calculation. The first and second peaks of the auto-correlation function are separated by $\sim 0.2\,\mathrm{s}$, in excellent agreement with presence of power at a frequency $\approx 5\ s^{-1}$ in the CLEAN result. Fig. 9 shows the corresponding CLEAN results for three selected 2D models. Since, as discussed in Sec. 3.1, there are two eddy turnovers during one period, we expect the power to be concentrated at low frequencies corresponding to one (half period) and two (full period) eddy turnover times. This expectation is confirmed, as can be seen in Fig. 9.

This period determination is consistent with the time for the flame "brush" to travel the distance between the vortex streets left in the bubble wake. In the particular case shown in Fig. 3, the distance between two consecutive, countervailing vortex streets is $\sim 2.7 \times 10^6$ cm (this can also be measured in the bottom panels of Fig. 3 more easily), while the flame sweeps through the computational domain with total speed $\sim 1.5 \times 10^7$ cm/s.[5]

Our results in this section lead to the conclusion that the semi-periodic behavior we observe is caused by the turnover of the largest eddies present in the simulation. This behavior is clearly visible in 2D simulations. In the supernova setting, a steady state realized in our model flame study is, strictly speaking, not present due to supernova expansion that makes both gravity and pre-flame conditions time-dependent. Therefore, supernova flame never achieves steady state but rather constantly struggles to approach that (now) time-dependent condition. One may expect that in that case a semi-periodic behavior exhibited by model flames might be significantly weaker or perhaps even completely suppressed (depending on whether flame evolution proceeds on timescales short compared to that of the background expansion).

[5] The total speed is the sum of the turbulent flame speed, $\sim 0.8 \times 10^6$ cm/s (Fig. 2), and the mean fluid velocity, $\sim 0.7 \times 10^6$ cm/s.

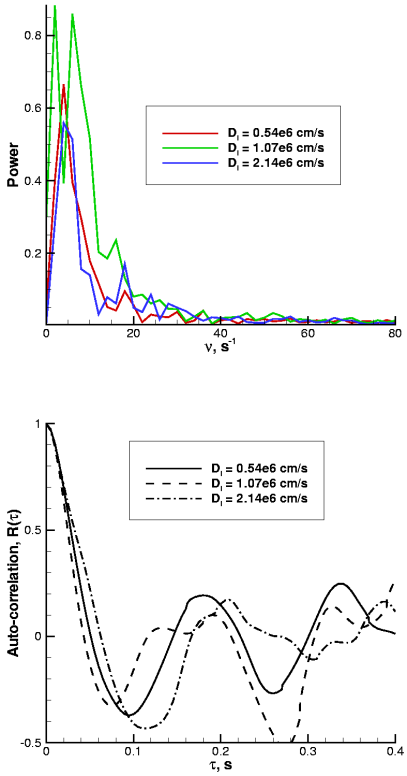

FIG. 8.— Time scales for the evolution of turbulent flames. The CLEAN power spectrum (left) and the auto-correlation function $R(\tau)$ (right) are plotted for the 3D time series data shown in Fig. 2. In the first panel, the power peaks at a frequency of $\approx 5\ s^{-1}$. This is consistent with the separation of the first and the second peak of the auto-correlation by $\approx 0.2\,\mathrm{s}$.

3.3. *Governing Equation for Flame Surface Area Evolution*

As previously mentioned, Khokhlov (1995) suggested that the flame surface evolution is governed by Eq. (3). The first term on the right-hand side of this equation describes flame surface creation via strain, while the second term describes flame surface destruction due to the propagation of cusps. Khokhlov (1995) motivated a general S^2 dependence of the flame surface destruction term by considering elemental geometries such as intersecting spheres and parallel planes.

To determine whether the flame surface destruction term in (3) is indeed proportional to S^2 let us consider the following generalized equation:

$$\frac{dS}{dt} = aS - bS^n\,, \tag{5}$$

where $a = c$ and $b = dD_l$ are arbitary constants for the moment, and $n > 0$. A steady state (equilibrium)

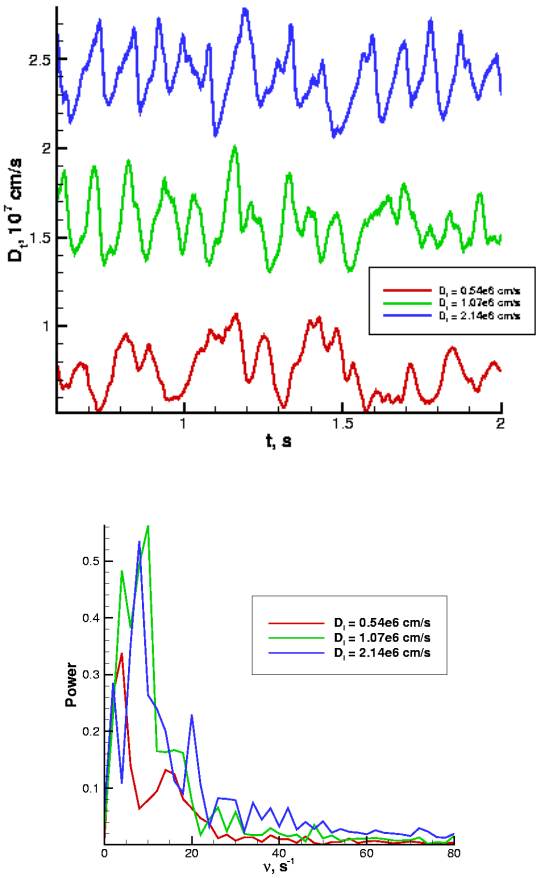

FIG. 9.— Evolution of the turbulent flame speed, D_t in 2D in steady state (left panel) and the corresponding CLEAN power spectrum (right panel). Note that offsets of 0.9×10^7 and 1.8×10^7 cm/s have been added to the slowest and the second slowest laminar flame speed cases, respectively.

solution, S_e, to (5) can be found by equating the creation (first) and destruction (second) term to produce,

$$S_e = \left(\frac{a}{b}\right)^{\frac{1}{n-1}}. \tag{6}$$

Now, let us add a constant perturbation Δa to the surface creation coefficient, a, to obtain a new equilibrium solution S'_e as,

$$S'_e = \left(\frac{a+\Delta a}{b}\right)^{\frac{1}{n-1}} = \left(\frac{a}{b}\right)^{\frac{1}{n-1}} \left(1+\frac{\Delta a}{a}\right)^{\frac{1}{n-1}}, \tag{7}$$

Therefore, the difference between the two equilibrium solutions is

$$\begin{aligned} \Delta S &= S'_e - S_e \\ &= \left(\tfrac{a+\Delta a}{b}\right)^{\frac{1}{n-1}} - \left(\tfrac{a}{b}\right)^{\frac{1}{n-1}} \\ &= \left(\tfrac{a}{b}\right)^{\frac{1}{n-1}} \left[\left(1+\tfrac{\Delta a}{a}\right)^{\frac{1}{n-1}} - 1\right]. \end{aligned} \tag{8}$$

In the limit of $\frac{\Delta a}{a} \ll 1$, Eq. (8) yields

$$\Delta S = \frac{\Delta a}{(n-1)a}\left(\frac{a}{b}\right)^{\frac{1}{n-1}}. \tag{9}$$

¿From this one can see that for a given a, b and $n > 1$, the magnitude of ΔS is proportional to Δa. Also, for a given a, Δa and $n > 1$, ΔS is proportional to $\left(\frac{1}{b}\right)^{\frac{1}{n-1}}$.

Let us now consider a time-dependent perturbation, $\Delta a(t)$, and ask if the above properties still obtain under this generalization. Assume

$$\Delta a(t) = \Delta a_0 \sin(\omega t), \tag{10}$$

where Δa_0 and ω are the amplitude and frequency of the perturbation, respectively. We have obtained numerical solutions for $a = 2$ and $\Delta a_0 = 0.2$. Three different values of n and b (equivalently, the laminar flame speed) were examined to determine the dependence of the equilibrium solution, S_e, and the deviation from it, ΔS, on n and b. Fig. 10 shows these solutions. The dependences of S_e and ΔS on n and b described by Eqs. (6) and (9) remain the same under the generalization of perturbation. Specifically, for a given a and Δa_0, we always obtain

$$S_e = \left(\frac{a}{b}\right)^{\frac{1}{n-1}} \tag{11}$$

$$\Delta S = \frac{\Delta a_0}{(n-1)a}\left(\frac{a}{b}\right)^{\frac{1}{n-1}}. \tag{12}$$

With these two functional dependences firmly established, we are left with determining the value of n in (5) to completely specify the governing equation of the flame surface area evolution.

As was demonstrated in Sec. 3.1, both the time-averaged value and the standard deviation of the flame surface area is proportional to $1/D_l$. Eqs. (11 and (12 then imply that n, in Eq. (5) is indeed equal to 2. (A new subgrid model can then be developed based on Eq. (3) of the flame surface area evolution. Details of the new model will be discussed in a forthcoming paper.) Therefore, we restrict our immediate discussion to the case $n = 2$. Note that we assume the creation coefficient, a, and its deviation, Δa_0, are constant for different laminar flame speed, D_l's. We will provide evidence that this is a reasonable assumption in the following section.

In case $n = 2$, Eqs. (11) and (12) yield

$$S_e = \frac{a}{b}, \tag{13}$$

$$\Delta S = \frac{\Delta a_0}{b}. \tag{14}$$

The amplitude of the variation of the flame surface area, S, in the steady state is proportional to the amplitude of the variation of the perturbation, Δa_0. Intuitively, there should exist a relaxation time scale, τ_r, associated with the response of S to a perturbation in the creation coefficient, a. For $a = $ const, the solution of Eq. (5) is

$$S = \frac{S_0 S_e}{S_e e^{-at} + S_0(1-e^{-at})}, \tag{15}$$

and can be also written as

$$\frac{a-bS}{bS} = \frac{S_e - S}{S} = \frac{S_e - S_0}{S_0} e^{-at}, \tag{16}$$

where $S_0 = S(t=0)$. Therefore, the relaxation time scale τ_r is determined solely by the value of the coefficient

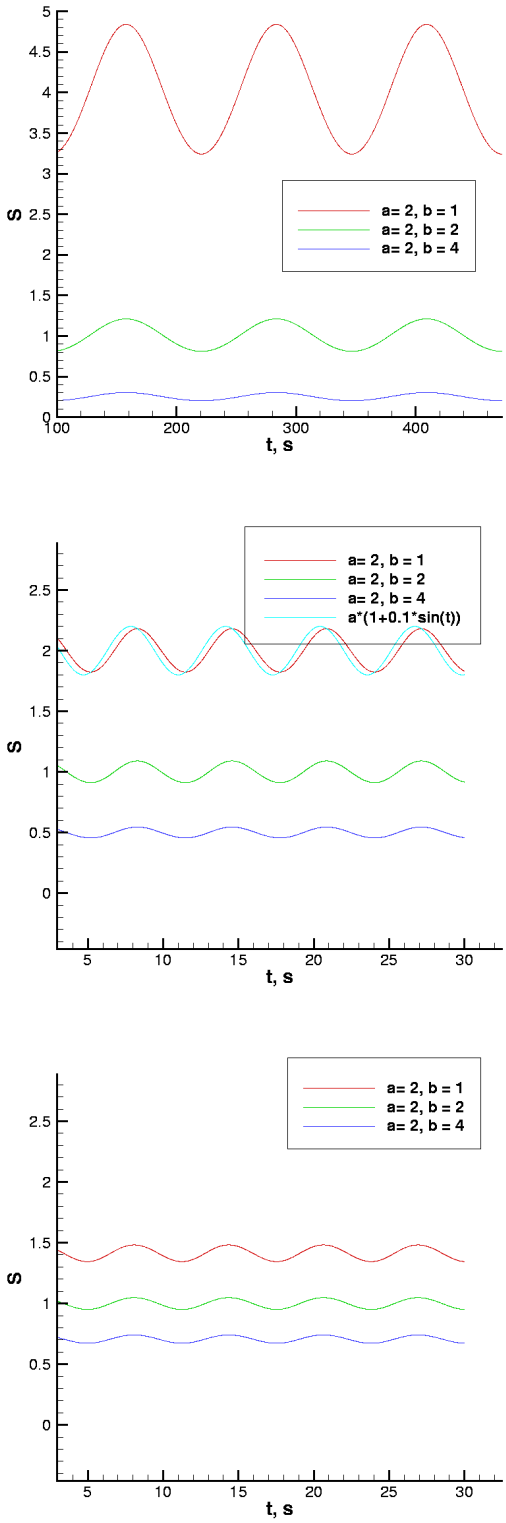

FIG. 10.— Solution of Eq. (5) with different b and n's. Top: $n = 1.5$; middle: $n = 2$; Bottom: $n = 3$. Creation = a(1. + 0.1sin(ωt))S for all cases.

a itself. For specificity, let us assume $\tau_r = 1/a$. Note that this relaxation time scale does not depend on b (or, equivalently, the laminar flame speed). We can see from Fig. 10 that, for the perturbation defined in Eq. (10), there is no phase difference between cases with different laminar flame speed. The difference in laminar flame speed affects only the steady state value of S and the deviation from it.

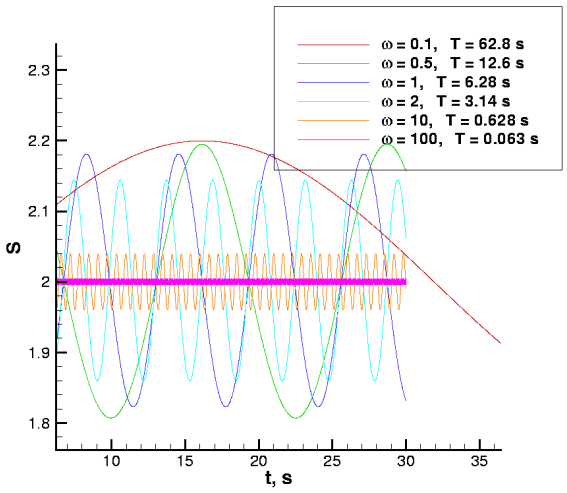

FIG. 11.— Solution of Eq. (5) for several values of ω. a =2, b =1, and $\Delta a_0 = 0.2$ for all cases. Note the percentage variation in flame surface area, S, is close to 10% only when the period of excitation, T, is small compared to the relaxation time scale $\tau_r = 1/a = 0.5$ s.

Given that it takes some time for the flame surface to respond to a change in the flow conditions, we might expect the variation of the flame surface area to be different when the frequency of the excitation, ω, in Eq. (10) changes. To examine the response of the flame surface area to excitations of different frequencies, a numerical experiment was performed with $a = 2$, $b = 1$ and $\Delta a_0 = 0.1a = 0.2$. The frequency of the excitation is varied from 0.1 to 100 s^{-1}. Combining Eqs. (13) and (14), we obtain

$$\frac{\Delta S}{S_e} = \frac{\Delta a_0}{a},$$

i.e., the percent variation in the flame surface area is equal to the percent variation of the creation coefficient. It is clear from Fig. 11 that only when the frequency of excitation is low ($\omega < 1$) is the amplitude of the variation in S as large as the percentage variation of the creation coefficient, *i.e.* ∼10%. When the frequency of excitation is large ($\omega > 1$), the flame surface becomes less responsive and the percentage by which the flame surface area varies decreases to below 10%. The relaxation time scale in this case is $\tau_r = 1/a = 0.5$ s. The period of excitation, T, is 6.28 s for an excitation frequency of 1 s^{-1}. Therefore, the period of excitation needs to be about ten times larger than the relaxation time scale for the flame surface to "fully" respond to the excitation.

3.4. *Flame Surface Creation and Destruction*

After determining the form of the governing equation of the flame surface area evolution, let us now attempt to determine the parameters in the equation for the actual physical system.

As introduced at the beginning of Sec. 3, the evolution of the creation coefficient, c, is followed in terms of its average value, $\int_\Omega c dV / \int_\Omega dV$, where Ω is the total volume containing flame surface, *i. e.* all of the computational cells that contain flame surface. Fig. 12

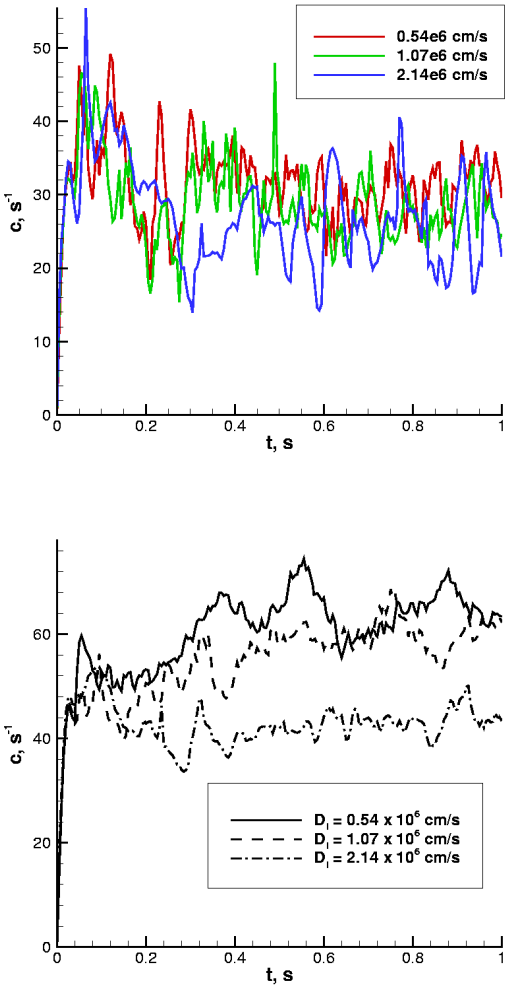

FIG. 12.— The temporal evolution of the surface creation in 2D (left) and 3D (right) in models DH, R1 and D2 and their counterparts in 2D. Note the similar time averaged value of c at different laminar flame speeds.

shows the evolution of the average creation coefficient for models DH, R1 and D2. One can see that c varies around 30 s^{-1} in 2D and 60 s^{-1} in 3D at different laminar flame speeds.[6] As discussed in the previous section, the reciprocal of the creation coefficient, $a = c$, is the relaxation time scale (τ_r) of flame response to a change in the flow conditions. The relaxation time scale is ≈ 0.033 and 0.017 s, in these models for 2D and 3D, respectively, while the RT time scale, $\tau_{RT} = \sqrt{L/Ag}$, is 0.05 s. In addition, $c \approx 50$ s^{-1} in a model with nominal gravity while about twice smaller than that in the model with gravity 4 times lower (see Fig. 13).

[6] Note the lower creation coefficient in the D2 run, where the flow field is not quite as turbulent as the other runs (*cf* Figs. 5 and 6).

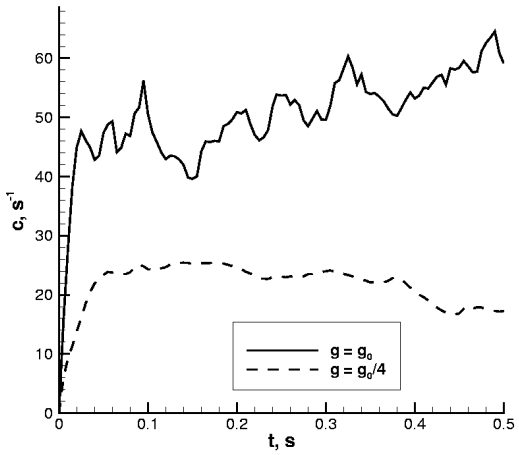

FIG. 13.— The temporal evolution of the surface creation coefficient in 3D models with nominal (solid) and 4 times lower gravity (dashed).

Therefore, the reciprocal of the creation coefficient seems to also be a measure of the RT time scale. This is actually the physical explanation for the independence of the relaxation time scale from the laminar flame speed discussed in the previous section.

It is also interesting to note that the creation coefficient in 3D is about twice as large as that in 2D. It can be shown analytically that the creation coefficient for a uniformly expanding sphere is twice as large as that of an expanding cylinder. It appears this effect of dimensionality can be generalized to more generic shapes. The additional potential for surface area creation afforded by an additional dimension also serves to explain why our determined turbulent flame speeds are roughly twice larger in 3D than in 2D (*cf* Figs. 2).

The numerical value of the surface destruction coefficient, d, can be estimated from the simulation data using Eq. (3). We obtain the destruction term by subtracting the rate of change of the flame surface area from the flame surface creation term. d is then obtained by dividing the destruction term by $D_l S^2$. Dimensional analysis indicates that the coefficient d must have the dimensions of specific volume. It is therefore reasonable to expect that d scales as $1/L^3$, where L is the lateral extent of the computational domain. To verify this result, we calculate three models of turbulent flame evolution in boxes of different lateral dimension, each model having lateral extent twice that of its predecessor (models LH, R1 and L2). The evolution of the destruction coefficient in those runs is shown in Fig. 14,

which clearly indicates that the destruction coefficient scales with the inverse of the simulation volume, *i.e.* $d \propto 1/L^3$. Given that the Rayleigh-Taylor bubble volume is comparable to L^3 at late times (Fig. 15), one can state that the destruction coefficient scales with the inverse of the characteristic Rayleigh-Taylor bubble volume.

The following interpretation of destruction coefficient scaling with the inverse of the Rayleigh-Taylor bubble volume can be offered:

Consider a box of size L per dimension filled with segments of flame surface. Let us assume that the segments

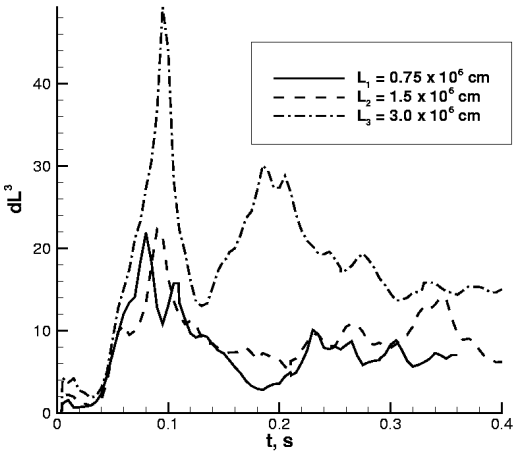

FIG. 14.— Comparison of the time evolution of dL^3 in models LH, R1 and L2, where d is the destruction coefficient and L is the lateral extent of the computational domain. Note that the destruction coefficient scales roughly as $1/L^3$.

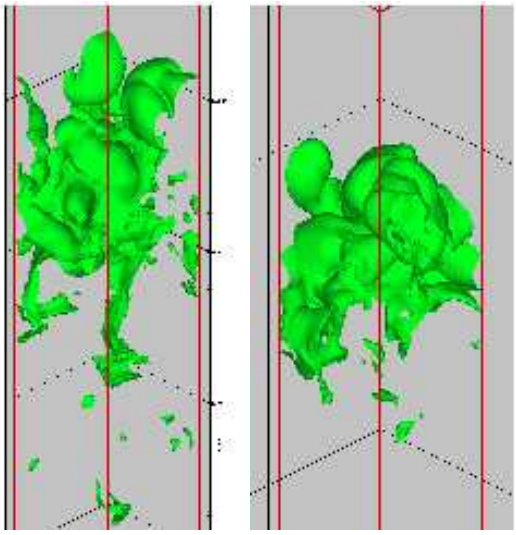

FIG. 15.— Morphology of the turbulent flame surface in models with different domain sizes at late times. (left) model R1: $L = 1.5 \times 10^6$ cm; (right) model LH: $L = 0.75 \times 10^6$ cm. Note that at late times the bubble size, l, becomes comparable to the size of computational domain, L.

are parallel to each other and are separated by distance Δ. Moreover, let us assume that the neighboring flame segments are moving towards each other with a constant speed, D_l. Then the surfaces are destroyed in collisions at the rate

$$\frac{S}{\Delta/D_l} = \frac{S^2}{S\Delta/D_l}\,.$$

In this case, the destruction coefficient is

$$d = \frac{1}{S\Delta}\,,$$

which can been seen as a measure of how much flame surface can be packed into a given volume. The term $S\Delta$ can be identified with the bubble volume.

The fact that the destruction coefficient is inversely proportional to the bubble volume, combined with dimensional analysis of the surface area change rate equation strengthens our conclusion that the surface destruction term is indeed proportional to S^2, in agreement with the original proposal of Khokhlov (1995).

3.5. *Froude Number and the Self-Regulation Mechanism*

The flame surface creation and destruction processes reflect the interplay between the Rayleigh-Taylor instability and the tendency of the burning process to smooth the flame's surface. This interplay has been clearly illustrated in Fig. 6 where we show the flame surface in three models obtained with different laminar flame speeds. Model DH (left panel in Fig. 6) has the lowest laminar flame speed and develops a flame surface which is substantially more convoluted than in the remaining two cases where the laminar flame speed is higher (models R1 and D2, middle and right panel in Fig. 6, respectively). The flame surface is relatively smooth in high laminar speed model D2. This behavior is well characterized by the Froude number,

$$Fr = \frac{D_l^2}{gL}\,,$$

which is the only parameter required to completely characterize the behavior of our model flames provided the density is constant. In models with higher Froude number the flame surface smoothing due to burning is stronger, resulting in a less convoluted flame surface. Conversely, in models with lower Froude number, the flame surface is strongly convoluted. The burning rate, however, remains controlled by the self-regulation mechanism and is independent of Froude number (*i.e.* independent of the laminar flame speed).

¿From the point of view of flame surface creation processes, systems characterized by smaller Froude number are expected to have similar surface creation coefficients, independent of D_l as long as the RT time scale are similar (as seen in Fig. 12). However, the creation coefficient will become sensitive to the laminar flame speed once the Froude number is such that the flame speedup factor, *i.e.* the ratio of turbulent flame speed to the laminar flame speed, becomes less than ∼10 for 3D.

3.6. *Verification of the KSGS model*

3.6.1. *Numerical Convergence*

To examine the convergence behavior of our numerical flame models, we perform simulations at three different spatial resolutions (models R1, R2 and R3). Fig. 16

shows the evolution of the turbulent flame speed, D_t, in these three models. At sufficiently late times the flame speed exhibits variations of $\approx 15\%$ around a mean value of $\approx 1.6 \times 10^7$ cm/s, and the detailed behavior is remarkably similar in all three cases. (Note that, due to limited computing resources, the highest resolution calculation was stopped at $t \approx 0.5$ s. Nevertheless, even in this case the flame speed increase saturates at a similar level as in the two lower resolution cases.) We also find that at any given instant of time the total burned mass is similar in all three models.

Due to the inviscid nature of the Euler equations, the flow structure will depend on numerical resolution to a degree. This is illustrated in Fig. 17

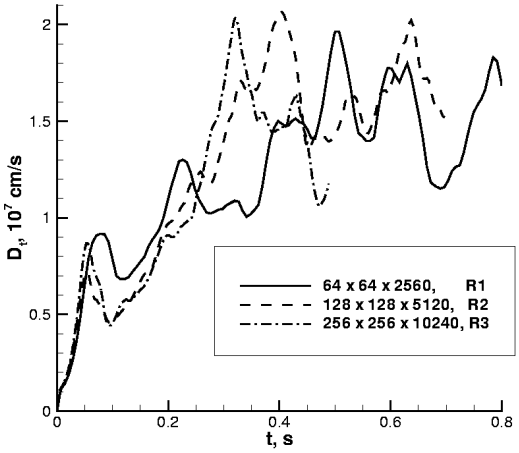

FIG. 16.— Convergence study for the turbulent flame models. Shown is the temporal evolution of the turbulent flame speed, D_t, in models R1, R2 and R3.

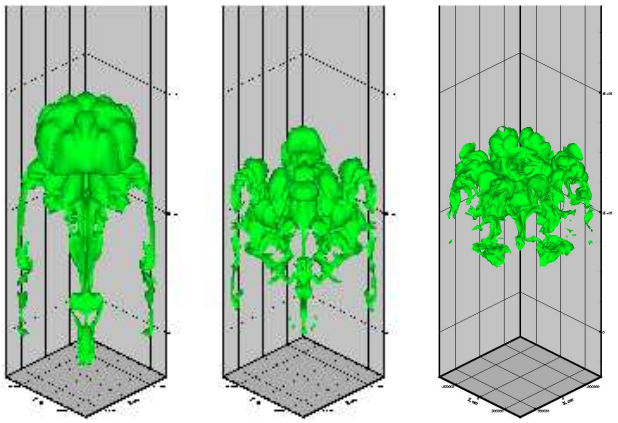

FIG. 17.— Dependence of the morphology of the turbulent flame surface on numerical resolution. The surface of the flame is shown at $t \sim 0.2\,\mathrm{s}$ in model R1 (left panel, $\Delta x = 2.34 \times 10^4\,\mathrm{cm}$), R2 (middle panel, $\Delta x = 1.17 \times 10^4\,\mathrm{cm}$) and R3 (right panel, $\Delta x = 5.86 \times 10^3\,\mathrm{cm}$).

where we show the morphology of the flame surface in models R1, R2, and R3 obtained at increasing resolution (but having fixed Froude number). One can notice a dramatic increase in the amount of small-scale structure as the resolution is increased. However, once the large scale characteristics of the flame are captured by the numerical model, the small scale structure emerging with increased numerical resolution does not change the global properties of the evolution, as seen in the convergence of the turbulent flame speed shown in Fig. 16.

Our results might also be expected to depend on certain technical aspects of the simulations. For example, due to the finite thickness of the numerical flame front it is desirable to study the dependence of our results on this numerical parameter. For this purpose we obtained models BH and B2, in which we adjust the nominal numerical flame thickness to, respectively, 0.75 and 1.5 times the standard value used in model R1. This is accomplished by changing the parameter b from 4 to 3 (model BH) or 6 (model B2). Figure 18

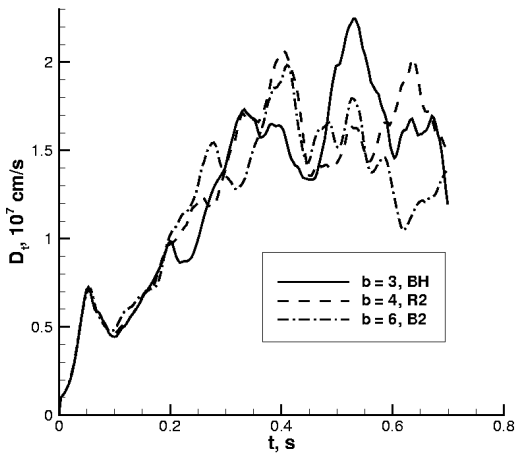

FIG. 18.— Dependence of the turbulent flame speed on the nominal numerical thickness of the flame front, b, in models BH, R2 and B2. Note that in all cases the turbulent flame speed oscillates around a similar average value.

shows that at late times the turbulent flame speed in all three models oscillates around a similar mean value with an amplitude entirely consistent with that observed in the resolution study discussed above.

Since our fiducial simulations make use of adaptive discretization, it is necessary to verify that local nonuniformity of the computational grid does not markedly influence the evolution of the system. Figure 19

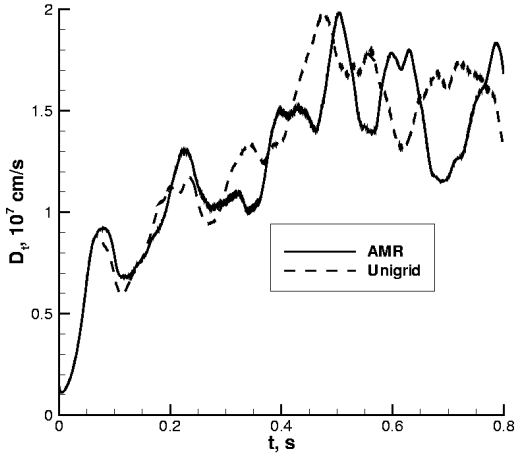

FIG. 19.— Verification of the adaptive mesh refinement model of the turbulent flame. Temporal evolution of the turbulent flame speed in the AMR model is plotted along that obtained in the simulation with uniform grid. The two models produce statistically similar results.

shows the evolution of the turbulent flame speed in model R1 and its counterpart calculation on a uniform mesh. The two models perfectly agree at very early times ($t < 0.1\,\mathrm{s}$) when the flame evolution remains confined

to the region initially refine. The two models begin to differ during the initial transient phase when the flame structure becomes progressively turbulent and the mesh in model R1 begins to follow the evolving flame structure. However, in steady state, the flame speeds in the two models saturate at similar levels. Also, we find that the power spectrum of the time variation of the flame surface area obtained in the model calculated on a uniform grid shows the same salient features (location of peak power, concentration at long timescales) as the AMR-enabled model.

3.6.2. *Examining the Self-Regulation Mechanism*

One of the main goals of this study is to verify the KSGS subgrid-scale model proposed by Khokhlov (1995). The KSGS model considers turbulence driven by the Rayleigh-Taylor instability on scales comparable to the grid resolution. In this model, the instantaneous turbulent flame speed, D_t, is

$$D_t = 0.5\sqrt{AgL}\,, \tag{17}$$

where $A = (\rho_0 - \rho_1)/(\rho_0 + \rho_1)$ is the Atwood number, ρ_0 and ρ_1 are the densities ahead and behind the flame front, respectively, g is the gravitational acceleration, and L is the turbulent driving scale, usually set to one or two computational cell widths in large-scale simulations making use of the KSGS model (Gamezo et al. 2003). A number of models were calculated to verify the applicability of Eq. (17) for different g and/or L . The results are shown in Fig. 20.

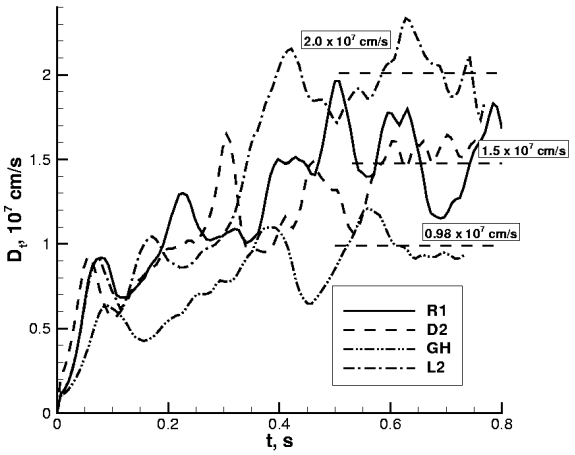

FIG. 20.— Verification of the KSGS model of RT-driven turbulent flames. The time evolution of the turbulent flame speed is shown for models R1 (reference model), D2 (twice laminar flame speed), GH (half gravitational acceleration), and L2 (twice larger domain size). Time averaged turbulent flame speeds in the steady-state regime are within 10% of the values predicted by Eq. (17).

The time-averaged steady-state turbulent flame speeds are entirely consistent with the predictions of Eq. (17).

Another aspect of the verification of the KSGS model is to confirm the independence of the self-regulation mechanism from details of the flame microphysics, *i.e.* on the laminar flame speed. To verify this, models DH, R1, and D2 were obtained for the same initial conditions and resolutions, but using laminar flame speeds differing by a factor of 2. The long-term evolutions of the turbulent flame speeds in these models are shown in Fig. 2, which clearly illustrates the expected independence of the turbulent and laminar flames speeds.

4. SUMMARY

We present the results of an extensive study of the evolution of thermonuclear flames in periodic domains under the influence of a constant gravitational field. The flame surface is Rayleigh-Taylor unstable, leading to a growth of initial perturbations. We follow the flame's development through an extended initial transient phase and find a well-defined steady-state regime. We verify that the evolution of RT-unstable flames is self-regulated, *i.e.* the turbulent flame surface evolution in steady state is independent of the details of the incorporated microphysics.

The evolution of the flame surface was examined. The functional dependence of flame surface destruction suggested by (Khokhlov 1995) is proven and the properties of the governing equation of the surface evolution are discussed. The flame surface creation coefficient is found to be closely related to the RT time scale and the flame surface destruction strength is found to vary as $1/L^3$, where L is the turbulent driving scale. The flame surface creation and destruction processes reflect the interplay between the Rayleigh-Taylor instability and the flame's tendency to smooth its surface. We find this relationship can be well characterized by the Froude number.

We find that the turbulent flame speed obeys a $\sqrt{AgL}$ scaling law for Froude numbers $\ll 1$. Also, we are able to identify semi-periodic temporal variations in the flame evolution in steady state and associate them with the turnover time of the largest eddies; no significant amount of power on shorter time scales is found, indicating the evolution is governed by large-scale flow characteristics.

We discussed in some detail the mechanism of vorticity generation, shedding, and transport in the vicinity of the flame surface. We find that the interaction between induced vorticity and the flame surface plays an important role in the flame evolution, leading to bubble "wobbling" on timescales comparable to the eddy turnover time. As the bubbles rise, vorticity is advected downstream into the bulk and forms an homogenized, mixed turbulent layer. It is in this layer where most of the flame surface destruction takes place. Although there exisst noticeable differences between flame dynamics in 2D and 3D, the vorticity production and advection, as well as the interaction between vortices and the flame surface appear quite generic.

There are several possible future directions of research emerging from our study. Our convergence study indicates that the self-regulation mechanism is relatively insensitive to the numerical resolution, provided the driving scales are adequately resolved. However, at the highest tested resolutions, we exhaust our current computing resources and are unable to investigate evolution with the Gibson scale fully resolved. Such investigation, bridging large and small scales in one model, is highly desirable. A full 3D implementation and tests including large-scale Type Ia simulations with a new subgrid model will also be conducted.

This work is supported in part by the U.S. Department of Energy under Grant No. B523820 to the Center for Astrophysical Thermonuclear Flashes at the University of Chicago. This research used resources of the National Energy Research Scientific Computing Center, which is supported by the Office of Science of the U.S. Department of Energy under Contract No. DE-AC03-76SF00098, and of the Teraport project at the University of Chicago through National Science Foundation Grant No. 0321253. We would also like to thank Timur Linde for implementing the marching cubes module in FLASH and Janusz Kałużny for making implementation of the CLEAN algorithm available to us.

APPENDIX

In order to verify the correctness and applicability of the CLEAN algorithm implementation, we have generated and analyzed a set of trial time series. The first test time series consists of single frequency signal with $\nu = 19.5$ s^{-1}. Figure 1

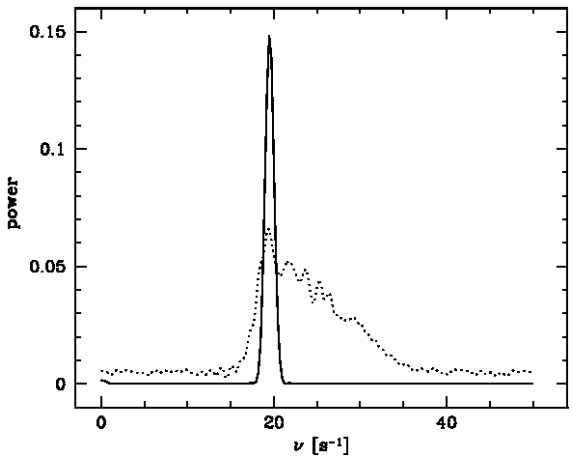

FIG. 1.— CLEAN power spectrum of trial time series with single frequency without (solid) and with (dotted) frequecy drift. See text for details.

shows that this single frequency is clearly identified by CLEAN (solid line). We can extend this trivial example to consider the effect of frequency drift on our ability to identify the spectrum. In a second test the time variable is transformed using a simple power-law, $t^{(0.9+0.2\times(t/t_e))}$, where t_e is the final time. The resulting power spectrum is shown in Fig. 1 (dotted line). The power now occupies a much wider range of frequencies, consistent with the assumed drift of the base frequency. We posit that such a drift around a base frequency occurs in the complex interaction between the RT-unstable flame with its own induced turbulent velocity field. This leads to a substantial leakage of power to frequencies neighboring the characteristic RT (turnover) frequency.

In another verification test, the trial signal consists of multiple discrete frequencies superposed on a white noise signal:

$$s(t) = A_0 r_0(t) \sum_{i=1}^{N} A_i[1 + r_i(t)] \cos(\pi\nu_i(2t + 10^{-2} r_i'(t))),$$

where $N = 4$, $r_{\{0,i\}}$ and r' are time-dependent random numbers between -1 to 1, (A_i, ν_i) (chosen to be are (0.1,4), (0.1,5), (0.3,19.5), (0.1,38)) are the amplitudes and matched frequencies of the discrete signals, respectively, and the amplitude of the white noise is $A_0 = 0.1$. The time series consisted of 100 equally spaced points in time between 0 and 1. Despite the fact that (a) some frequencies are closely spaced and/or aliased, (b) the amplitude of white noise is comparable to that of the composite signals, and (c) small random perturbations have been added in the time domain, most all the informational content in the signal is identified by the CLEAN method (Fig. 2).

Only in the case of the two lowest closely-spaced frequencies (ν =4,5) does the method fail to clearly delineate the separate signals. Even in this case the power peak is relatively broad, suggesting the presence of distinct signals in the region.

REFERENCES

Arnett, W. D. 1969, Ap&SS, 5, 180
Arnett, W. D. 1974, ApJ, 191, 727
Clement, M. J. 1993, ApJ, 406, 651
Colella, P. & Woodward, P. R. 1984, J. Comput. Phys., 54, 174
Damköhler, G. 1939, Jahrb. Deut. Luftfahrtforsch., 113
Fryxell, B., et al. 2000, ApJS, 131, 273
Gamezo, V., et al. 2003, Science, 299, 77
Hoyle, P., & Fowler, W. A. 1960, ApJ, 132, 565
Khokhlov, A. M. 1995, ApJ, 449, 695
Lorensen, W. E. & Cline, H. E. 1987, Computer Graphics, 21 (4), 163
Müller, E., & Arnett, W. D. 1982, ApJ, 261, L109
Müller, E., & Arnett, W. D. 1986, ApJ, 307, 618
Niemeyer, J. C, & Hillebrandt, W. 1995, ApJ, 452, 769

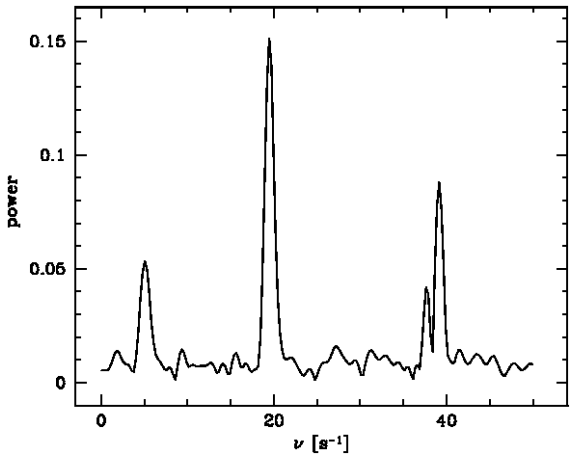

FIG. 2.— CLEAN power spectrum for signal with multiple, closely-spaced, and aliased frequencies in the presence of significant white noise. Note that all major component frequencies are clearly identified with the exception of the two low frequency signals (power peak around $\nu = 5\ \mathrm{s}^{-1}$).

Niemeyer, J. C., Hillebrandt, W., & Woosley, S. E. 1996, ApJ, 471, 903
Nomoto, K., Sugimoto, D., & Neo, S. 1976, Ap&SS, 39, L37
Nomoto, K., Thielemann, F.-K., & Yokoi, K. 1984, ApJ, 286, 644
Ostriker, J. P., Richstone, D. O., & Thuan, T. X. 1974, ApJ, 188, L87
Reinecke, M., Hillebrandt, W., & Niemeyer, J. C. 1999, A&A, 347, 724
Reinecke, M., Hillebrandt, W., & Niemeyer, J. C. 2002, A&A, 391, 1167
Roberts, D. H., Lehar, J., & Dreher, J. W. 1987, AJ, 93, 968
Schmidt, W., Niemeyer, J. C., Hillebrandt, W., & Röpke, F. K. 2006, A&A, 450, 283
Timmes, F. X., & Swesty, F. D. 2000, ApJS, 126, 501
Vladimirova, N., Weirs, V. G., & Ryzhik, L. 2006, Combustion Theory Modelling, in press.
Vladimirova, N., & Rosner, R. 2005, Phys. Rev. E, 71, 067303
White, F. M. 2003, Fluid Mechanics, published by MaGraw-Hill Companies.
Zhiglo, A. V. 2005, astro-ph/0511374